

**Supplementary Information For:**

**‘Colorful’ Polyline Grain Boundaries in Two-dimensional  
Transition Metal Dichalcogenides**

Maolin Yu<sup>1#</sup>, Chao Zhu<sup>2#</sup>, Yongmin He<sup>2</sup>, Jiadong Zhou<sup>2</sup>, Ying Xu<sup>1</sup>, Zheng Liu<sup>2,3\*</sup>, Wanlin Guo<sup>1\*</sup>,  
Zhuhua Zhang<sup>1\*</sup>

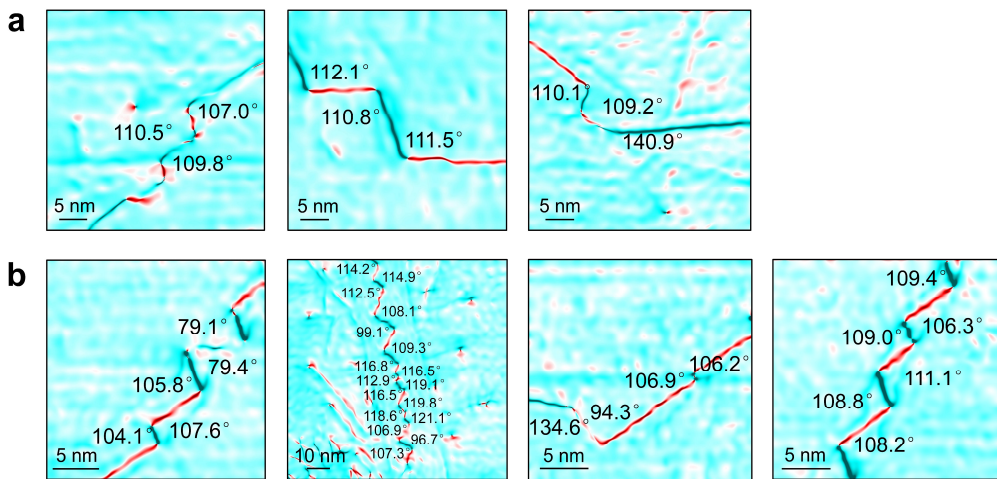
<sup>1</sup>*Key Laboratory for Intelligent Nano Materials and Devices of Ministry of Education, State  
Key Laboratory of Mechanics and Control of Mechanical Structures, and Institute of  
Nanoscience, Nanjing University of Aeronautics and Astronautics, Nanjing 210016, China.*

<sup>2</sup>*School of Materials Science and Engineering, Nanyang Technological University, Singapore  
639798, Singapore.*

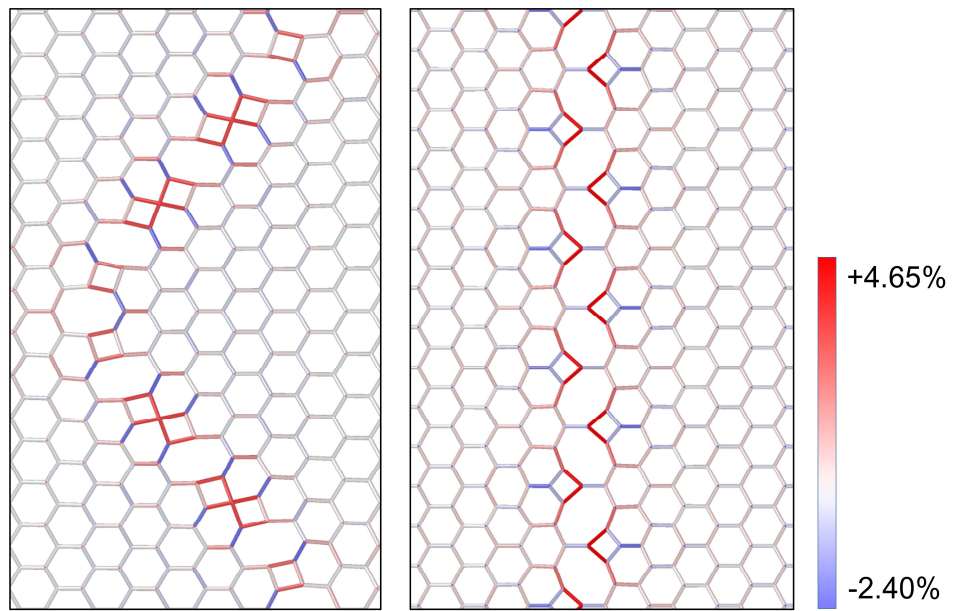
<sup>3</sup>*School of Electrical and Electronic Engineering, Nanyang Technological University,  
Singapore 639798, Singapore.*

<sup>#</sup>These authors contributed equally to this work.

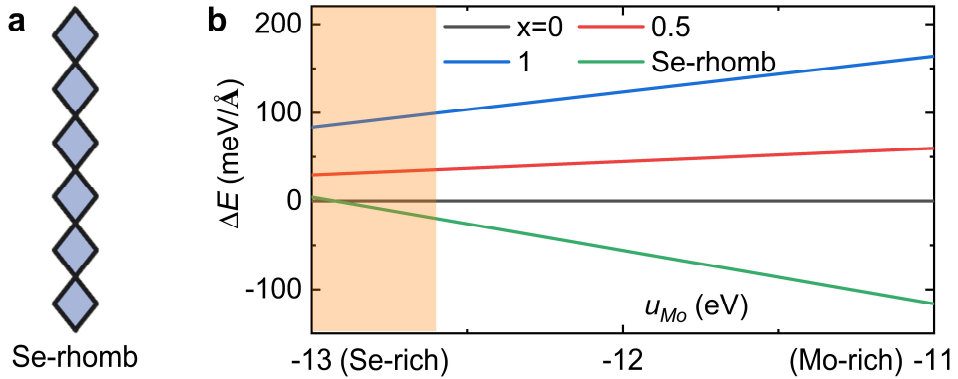
\*To whom correspondence should be addressed: Zheng Liu (z.liu@ntu.edu.sg); Wanlin Guo  
(wlguo@nuaa.edu.cn); Zhuhua Zhang ([chuwazhang@nuaa.edu.cn](mailto:chuwazhang@nuaa.edu.cn)).



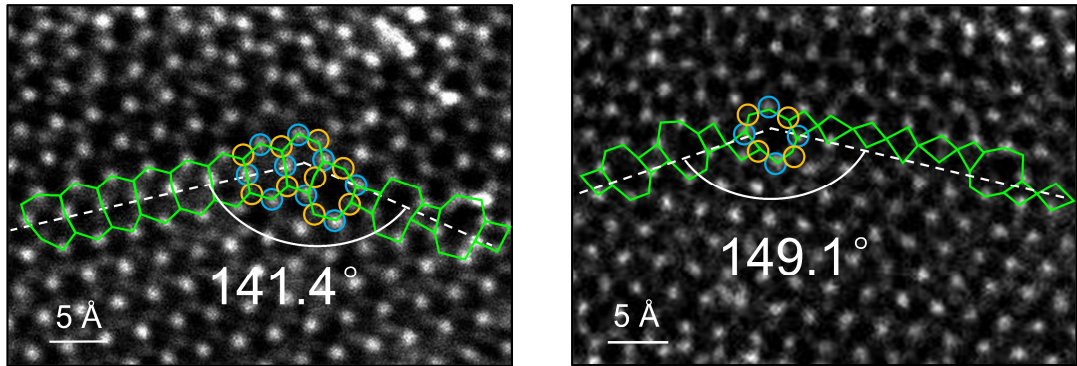
**Supplementary Figure S1. Adjunctive rotation maps of lattice along GBs in different samples.** **a**, The first three images are extracted from our experimental work. **b**, The last four images are adapted from ref. 24, Springer Nature Ltd.



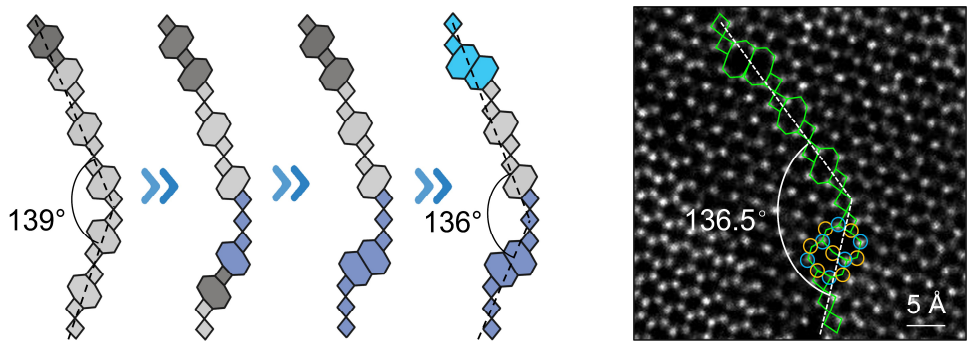
**Supplementary Figure S2. Calculated strain maps around the polyline and straight GBs, respectively.** Compared with Mo-4|8 structure that has the lattice strain concentrated along the GB in a range of -2.27 ~ 4.65%, the polyline one has a rather dispersive distribution of the in-plane strain field with distinctly smaller magnitudes ranged in -2.4 ~ 3.41%.



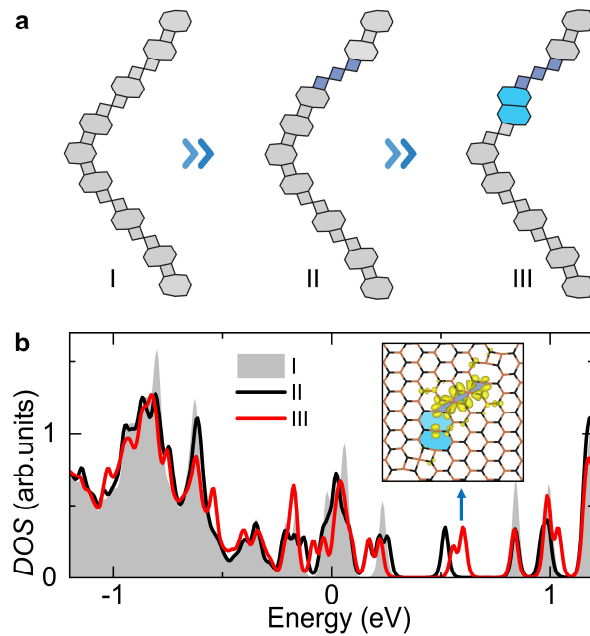
**Supplementary Figure S3. Energetic of the p-GBs with two segments misoriented by 120°.** **a**, A Se-rhomb structure with successive squares along the GB is built for comparison. **b**, Relative energy of those p-GBs in Figure 2d to the one with  $x = 0$  as a function of the chemical potential of Mo,  $\mu_{\text{Mo}}$ . Near the experimental Se-rich bound, most p-GB structures are still less stable than the straight Se-rhomb one.



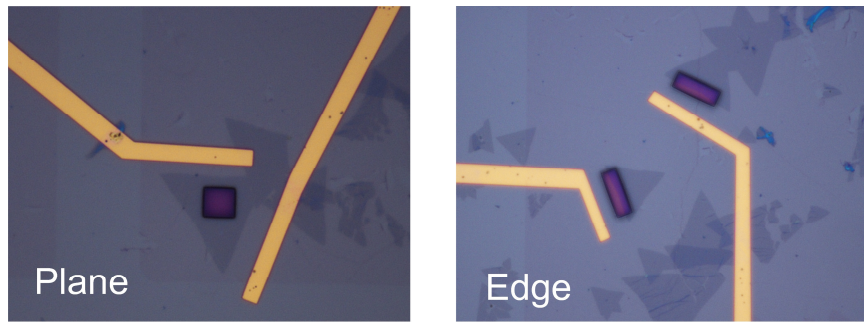
**Supplementary Figure S4. Atomic-resolution ADF-STEM images of selected GBs with  $\theta_f = 141.4^\circ$  and  $149.1^\circ$ , respectively.** Strings of successive squares and octagons are clearly observed in the two p-GBs with extremely high folding angles, respectively. These p-GBs will require the inclusion of one segment oriented exactly along the interstice between two zigzag edges that are antisymmetric to each other. These were only occasionally observed in our experiments, as proven by the statistics in Fig. 1b. The reason may lie in that the growth fronts of two inversely oriented domains can hardly fit each other along the zigzag line due to fluctuations of growth kinetics.



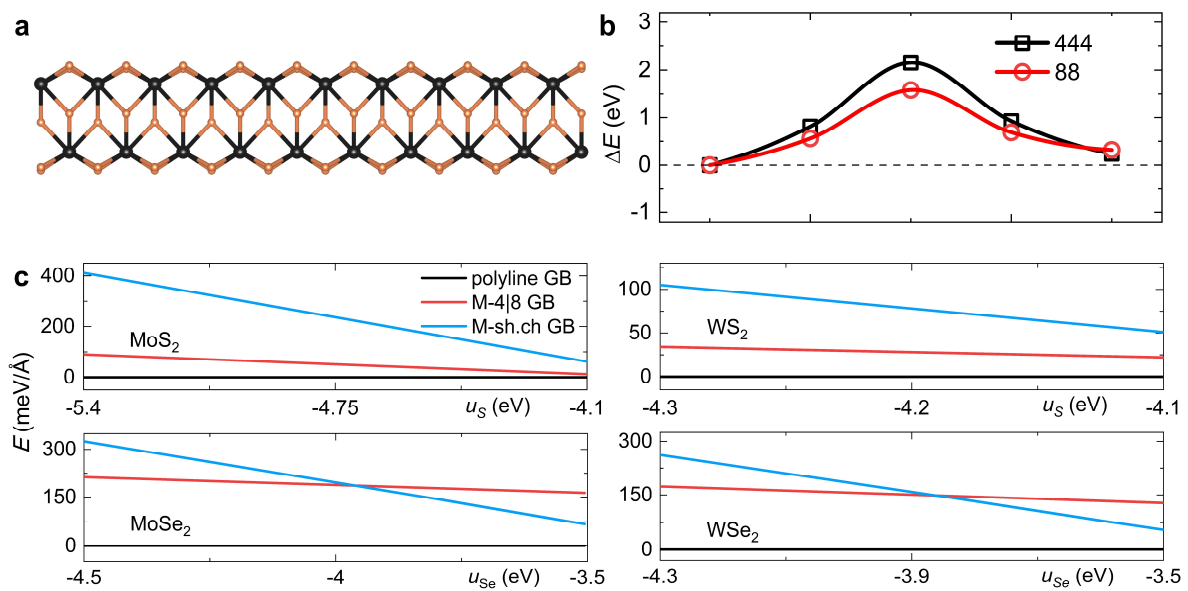
**Supplementary Figure S5. Evolution of the p-GB with  $x = 0.29$  and an initial  $\theta_f$  of  $139^\circ$  composed of misoriented octagons in two segments.** The light gray, dark gray, light blue, and dark blue segments represent the  $4|4|8$ ,  $4|8$ ,  $4|4|4|8$ , and  $4|4|8|8$  cores, respectively. Folding angles of the p-GB in the initial and final steps are marked. The final structure is verified by an experimental ADF-STEM image, which is the one shown in the rightmost of Fig. 1c.



**Supplementary Figure S6. Effect of polygon migrations on electronic properties of the p-GB.** **a**, Illustration for the selected steps of polygon migrations along a p-GB with  $x = 0.5$ . Polygons colored light and dark blue represent the  $8|8$  and  $4|4|4$  cores, respectively. **b**, Calculated DOS of the p-GBs at the three steps in (a) are shown by the shaded area, black and red lines, respectively. Inset shows an isosurface plot ( $0.03 \text{ e}/\text{\AA}^3$ ) of partial charge density corresponding to the energy window of  $0.55$ - $0.65$  eV above the Fermi level.



**Supplementary Figure S7. Optical images of micro-electrochemical devices.** These devices are based on basal plane and edges of 2D MoS<sub>2</sub> sheets, respectively, where the HER process occurs at the exposed windows as indicated by a dark frame.



**Supplementary Figure S8. Energetics and evolution of p-GBs in 2D MX<sub>2</sub> (M = Mo, W; X= S, Se).** **a**, A structure of M-sh.ch GB reported to be most stable in ref. 34. Considering the interlayer interactions on substrate, the domains on both sides of GB are fixed on the same plane. **b**, Calculated minimum energy pathways for a W atom migrating along GB segments made of the 4|4|8 (black line) and 4|8 (red line) cores, respectively. **c**, Relative energy  $\Delta E$  of straight M-4|8 and M-sh.ch structures to the p-GB with  $x = 0.5$  as a function of the chemical potential of X,  $\mu_X$ . All the polyline structures show higher stability than the corresponding straight ones.